

# Performance Analysis for Multi-Antenna Small Cell Networks with Clustered Dynamic TDD

Hongguang Sun<sup>†,§</sup>, Howard H. Yang<sup>‡</sup>, Xijun Wang<sup>\*</sup>, Chao Xu<sup>†,§</sup>, and Tony Q.S. Quek<sup>‡</sup>

<sup>†</sup>School of Information Engineering, Northwest A&F University, Yangling, Shaanxi, China

<sup>‡</sup>Information System Technology and Design Pillar, Singapore University of Technology and Design, Singapore

<sup>\*</sup>School of Electronics and Communication Engineering, Sun Yat-sen University, Guangzhou, Guangdong, China

<sup>§</sup>Key Laboratory of Agricultural Internet of Things, Ministry of Agriculture and Rural Affairs, Yangling, Shaanxi, China

**Abstract**—Small cell networks with dynamic time-division duplex (D-TDD) have emerged as a potential solution to address the asymmetric traffic demands in 5G wireless networks. By allowing the dynamic adjustment of cell-specific UL/DL configuration, D-TDD flexibly allocates percentage of subframes to UL and DL transmissions to accommodate the traffic within each cell. However, the unaligned transmissions bring in extra interference which degrades the potential gain achieved by D-TDD. In this work, we propose an analytical framework to study the performance of multi-antenna small cell networks with clustered D-TDD, where cell clustering is employed to mitigate the interference from opposite transmission direction in neighboring cells. With tools from stochastic geometry, we derive explicit expressions and tractable tight upper bounds for success probability and network throughput. The proposed analytical framework allows to quantify the effect of key system parameters, such as UL/DL configuration, cluster size, antenna number, and SINR threshold. Our results show the superiority of the clustered D-TDD over the traditional D-TDD, and reveal the fact that there exists an optimal cluster size for DL performance, while UL performance always benefits from a larger cluster.

## I. INTRODUCTION

To satisfy the unprecedented high demands of data traffic, network densification has been considered as one of the key technologies in 5G wireless networks [1], [2]. With the densely deployed small cell access points (SAPs), not only the cell coverage, but also the spatial reuse gain is significantly enhanced [3]. To further improve the network performance, the combination of SAPs and multiple-input multiple-output (MIMO) technology is promising, where the spatial multiplexing gain and/or diversity gain can be exploited [4]. However, the dense deployment of SAPs increases the variation of traffic demands among different cells, and the accommodation to traffic fluctuation is essential. Dynamic time-division duplex (D-TDD) has emerged as a potential solution to address the asymmetric traffic demands [5]. Different from conventional static time-division duplex (S-TDD), where all SAPs employ the same uplink/downlink (UL/DL) configuration, D-TDD can efficiently support the asymmetric traffic by allowing each SAP to dynamically adjust its UL/DL resources [6], [7]. However, the flexibility is achieved at the expense of two new types of inter-cell interference: the SAP-to-SAP interference and mobile user to mobile user (MU-to-MU) interference.

To reduce the inter-cell interference, cell clustering has been proposed as an effective approach [8]–[10]. With the cell

clustering scheme, small cells in close proximity are classified into the same cluster, and adopt S-TDD in a per-cluster basis. As such, SAPs within the same cluster synchronize their transmissions, and the SAP-to-SAP and MU-to-MU interference can be eliminated within the cluster. Although the benefit of cell-clustering scheme has been evaluated in heterogeneous network [8] or centralized radio access network (C-RAN) [9] via simulations, an analytical framework is essential to fully understand the performance of clustered D-TDD scheme, and capture the effect of key network parameters. However, the spatial randomness of node's geographical location and the resulting aggregated interference distribution within a given cluster, put rigorous challenges for the development of analytical framework [11].

With tools from stochastic geometry, prior works model node's spatial irregularity by using classic spatial point process like Poisson Point Process (PPP) in D-TDD networks, without considering the cell clustering interference mitigation scheme [12], [13]. The authors in [10] first model the cell clustering scheme in a single-antenna small cell D-TDD network, and use an approximation approach to compute the aggregated interference from different clusters. With the extensive use of multi-antenna technique, the multi-antenna small cell network with clustered D-TDD is a promising architecture. In such a network, an analytical framework is required to characterize the synergy of cell clustering and multi-antenna techniques, so as to provide guidelines for the network design. However, to the best of our knowledge, there is no previous literature evaluating the D-TDD network by jointly considering the multi-antenna and cell clustering techniques.

In this work, we develop an analytical framework to study the performance of multi-antenna small cell networks operating clustered D-TDD. We model the SAP and MU locations as two independent PPPs, and form each cluster as a hexagon. Zero-forcing (ZF) beam-forming technique is considered for both DL and UL transmissions to cancel the inter-user interference within each cell. To reduce the computational complexity, we use an approximate method to calculate the aggregated interference, and derive tractable tight upper bounds for success probability and network throughput. The proposed analytical framework allows to characterize the effect of key network parameters, and provides guideline for the optimal design of cell clustering scheme.

## II. SYSTEM MODEL

### A. Network model

We consider a small cell network operating clustered D-TDD scheme, where the spatial locations of SAPs and MUs follow two independent homogeneous PPPs  $\Phi_s$  and  $\Phi_u$  with intensities  $\lambda_s$  and  $\lambda_u$ , respectively. We adopt the nearest association policy where each MU connects to its closest SAP. Let  $n \in \{0, 1, \dots, N\}$  be the number of MUs associated with each SAP where we limit the maximum number of MUs served by each SAP to  $N$ . According to the nearest association policy, the probability density function (PDF) of the distance from a MU to its associated SAP can be derived as  $f_r(r) = 2\pi\lambda_s r \exp(-\pi\lambda_s r^2)$  [14]. Each SAP is equipped with  $M$  antennas, while each MU has a single antenna. The transmit power of SAP (to each MU) and MU are defined as  $P_s$  and  $Q_u$ , respectively. The channel model consists of two attenuation components, namely large-scale pathloss, and small-scale Rayleigh fading. Specifically, the pathloss function is given by  $g(\|x\|) = \frac{1}{\|x\|^\alpha}$  with  $\alpha > 2$  being the pathloss exponent, and the small-scale Rayleigh fading with unit mean is given by  $h \sim \exp(1)$ .

### B. Transmission Scheme

In this network, we consider a fully-loaded model where each SAP always has data to transmit to all its associated MUs. We adopt the space division multiple access (SDMA) scheme, where the maximum number of MUs (associated to each SAP)  $N$  does not surpass the number of antennas  $M$ , i.e.,  $N \leq M$ . As a result, all the MUs can be served by its associated SAP simultaneously. To cancel the inter-user interference, we adopt ZF pre-coding at the DL SAPs, and ZF receiver at the UL SAPs with perfect knowledge of the channel state information (CSI). As such, the channel power gain between an SAP and an MU is different when the SAP acts as a serving SAP or interfering SAP in both DL and UL mode, which is discussed in more details in Section III.

### C. Cell Clustering Scheme

To reduce the interference from the opposite transmission direction, the cell clustering scheme is adopted where we group Voronoi cells that are closely located into clusters and align the transmissions in each cluster, as depicted in Fig. 1.

To cover the whole network region without overlap, we form each cluster as a hexagon. We define  $C(T, \rho)$  as a hexagon centered at  $T$  with  $\rho$  being the cluster radius (from the hexagon center  $T$  to the boundary). The area of  $C(T, \rho)$  can be easily calculated as  $2\sqrt{3}\rho^2$ , and the cluster size, i.e., the average number of SAPs per cluster, is given by  $l = 2\sqrt{3}\rho^2\lambda_s$ . Note that the cluster size  $l$  determines the operation pattern and interference mechanism of the whole network. Obviously, as  $l \rightarrow \infty$ , the network degenerates into operate under S-TDD scheme where all SAPs have the same transmission direction, while  $l \rightarrow 1$  leads to the traditional D-TDD scheme where each SAP individually sets its UL/DL configuration. With the proposed cell clustering scheme, SAPs within the same cluster

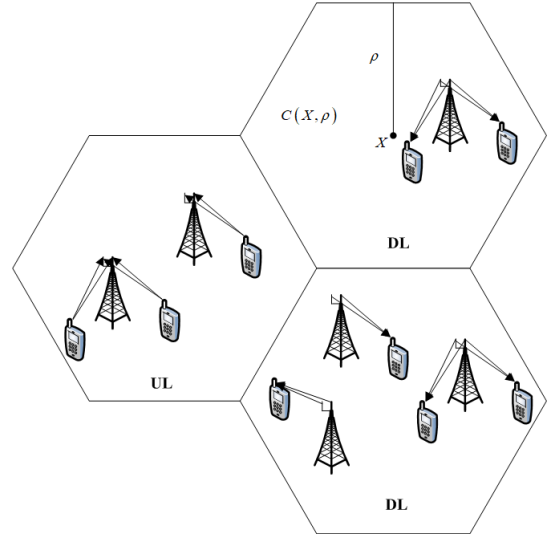


Figure 1. An illustration of clustered D-TDD for two-antenna small cell networks with  $\rho$  being the cluster radius, where SAPs located within the same cluster simultaneously align their UL/DL configurations at each time slot.

configure in DL (resp. UL) transmission with probability  $p_D$  (resp.  $1 - p_D$ ).

## III. PERFORMANCE ANALYSIS

### A. Success Probability

We consider the constant bit-rate coding, and define  $\gamma_D$  and  $\gamma_U$  as the DL and UL SINR thresholds. With the Sliviyark's theorem [15], [16], it is sufficient to focus on the SINR of a typical MU or SAP that locates at the origin. The success probability is defined as

$$\mu_{\text{TX}} \triangleq \Pr(\text{SINR}_{\text{TX}} > \gamma_{\text{TX}}), \text{TX} \in \{\text{D}, \text{U}\}. \quad (1)$$

With the cell clustering scheme, for a generic cluster, we can divide the locations of SAPs  $\Phi_s$  (resp. MUs  $\Phi_u$ ) into two independent PPPs  $\Phi_s^{\text{in}}$  and  $\Phi_s^{\text{out}}$  (resp.  $\Phi_u^{\text{in}}$  and  $\Phi_u^{\text{out}}$ ), which lie within intra-cluster zone and cross-cluster zone, respectively. By limiting the maximum number of MUs served by each SAP to  $N$ , we can decompose  $\Phi_s^{\text{in}}$  and  $\Phi_s^{\text{out}}$  into  $N$  tiers where the  $n$ -th ( $n \in \{1, \dots, N\}$ ) tier is constituted by SAPs with exactly  $n$  associated MUs. According to this, we can model the spatial locations of SAPs (MUs) in the  $n$ -th tier as  $\Phi_{s_n}^{\text{in}}$  ( $\Phi_{u_n}^{\text{in}}$ ) and  $\Phi_{s_n}^{\text{out}}$  ( $\Phi_{u_n}^{\text{out}}$ ), respectively. To analyze the aggregated interference from cross-cluster zone, we approximate the cross-cluster zone into a sequence of disjoint hexagonal rings. Specifically, let  $C(T, \rho)$  be the cluster of the typical SAP or MU, the cross-cluster zone can be approximated by  $\{\mathcal{A}_k\}_{k=1}^{\infty} = \{C(T, \sqrt{k+1}\rho) \setminus C(T, \sqrt{k}\rho)\}_{k=1}^{\infty}$  [17] where the  $k$ -th hexagonal ring  $\mathcal{A}_k$  corresponds to the  $k$ -th cluster, and the area of  $\mathcal{A}_k$  is the same as  $C(T, \rho)$ , i.e.,  $2\sqrt{3}\rho^2$ . In the  $k$ -th ring, we define  $\Phi_{s_k}^{\text{out}}$  and  $\Phi_{u_k}^{\text{out}}$  as the spatial locations of SAPs and MUs, respectively, and we have

$$\Phi_s = \Phi_s^{\text{in}} \cup \Phi_s^{\text{out}} = \left( \bigcup_{n=1}^N \Phi_{s_n}^{\text{in}} \right) \cup \left( \bigcup_{k=1}^{\infty} \bigcup_{n=1}^N \Phi_{s_n}^{\text{out}_k} \right), \quad (2)$$

$$\Phi_u = \Phi_u^{\text{in}} \cup \Phi_u^{\text{out}} = \left( \bigcup_{n=1}^N \Phi_{u_n}^{\text{in}} \right) \cup \left( \bigcup_{k=1}^{\infty} \bigcup_{n=1}^N \Phi_{u_n}^{\text{out},k} \right). \quad (3)$$

For the typical MU located at the origin  $\mathbf{0}$  in DL mode, the received SINR can be expressed as

$$\text{SINR}_D = \frac{P_s r_0^{-\alpha} \|\mathbf{h}_{0,0}^\dagger \mathbf{w}_{0,0}\|^2}{I_D + \sigma^2}, \quad (4)$$

where  $\mathbf{h}_{0,0} \in \mathbb{C}^{M \times 1}$  and  $\mathbf{w}_{0,0} \in \mathbb{C}^{M \times n_0}$ , respectively, denote the channel vector and the ZF pre-coding matrix at the tagged DL SAP (to the typical MU), and  $I_D$  denotes the aggregated interference from DL SAPs and UL MUs, given by

$$\begin{aligned} I_D &= \sum_{n=1}^N \sum_{x_i \in \Phi_{s_n}^{\text{in}} \setminus \{x_0\}} P_s \|x_{0,i}\|^{-\alpha} |\mathbf{h}_{0,i}^\dagger \mathbf{W}_i|^2 \\ &+ \sum_{k=1}^{\infty} \left[ \mathbf{1}_{\{\text{TX=D}\}}^{\text{out},k} \sum_{n=1}^N \sum_{x_j \in \Phi_{s_n}^{\text{out},k}} P_s \|x_{0,j}\|^{-\alpha} |\mathbf{h}_{0,j}^\dagger \mathbf{W}_j|^2 \right. \\ &\left. + \mathbf{1}_{\{\text{TX=U}\}}^{\text{out},k} \sum_{n=1}^N \sum_{z_l \in \Phi_{u_n}^{\text{out},k}} Q_u \|z_{0,l}\|^{-\alpha} |h_{0,l}|^2 \right], \quad (5) \end{aligned}$$

where indicator functions  $\mathbf{1}_{\{\text{TX=D}\}}^{\text{out},k}$  and  $\mathbf{1}_{\{\text{TX=U}\}}^{\text{out},k}$  represent that the SAPs in the  $n$ -th cluster are configured in DL and UL direction, respectively. The first part, second part and last part in (5) denote the DL interference from intra-cluster zone, cross-cluster zone, and UL interference from cross-cluster zone, respectively. The channel vectors from the interfering DL SAP located at  $x_i$  and  $x_j$  are denoted by  $\mathbf{h}_{0,i} \in \mathbb{C}^{M \times 1}$  and  $\mathbf{h}_{0,j} \in \mathbb{C}^{M \times 1}$ , respectively. For the UL interfering MUs, the channel gain from  $z_l$  to the typical MU is denoted by  $h_{0,l} \sim \mathcal{CN}(0, 1)$ . We define  $\tilde{\mathbf{H}}_i = [\tilde{\mathbf{h}}_{0,i}, \dots, \tilde{\mathbf{h}}_{c,i}, \dots, \tilde{\mathbf{h}}_{n-1,i}]^\dagger \in \mathbb{C}^{n \times M}$  as the channel matrix between a DL interfering SAP and all the  $n$  associated MUs. The direction of each vector channel is represented by  $\tilde{\mathbf{h}}_{c,i} \triangleq \frac{\mathbf{h}_{c,i}}{\|\mathbf{h}_{c,i}\|}$ , where  $\|\cdot\|$  denotes the Euclidean norm. By using ZF pre-coding, the columns of the pre-coding matrix  $\mathbf{W}_i = [\mathbf{w}_{i,c}]_{1 \leq c \leq n} \in \mathbb{C}^{M \times n}$  are exactly the columns of the pseudo-inverse  $\mathbf{H}_i^\dagger \triangleq \tilde{\mathbf{H}}_i^\dagger (\tilde{\mathbf{H}}_i \tilde{\mathbf{H}}_i^\dagger)^{-1} \in \mathbb{C}^{M \times n}$ , where  $(\cdot)^\dagger$  and  $(\cdot)^\dagger$  represent the pseudo-inverse and conjugate transpose, respectively.

Let  $n_0 \in \{1, 2, \dots, N\}$  be the number of MUs associated with the tagged DL SAP. The desired channel power gain can be derived as  $h_{0,0}^D = \|\mathbf{h}_{0,0}^\dagger \mathbf{w}_{0,0}\|^2 \sim \Gamma(M - n_0 + 1, 1)$  [18], the DL interference channel power gain is given by  $g_{x_i, \text{SAP}}^D = |\mathbf{h}_{0,i}^\dagger \mathbf{W}_i|^2 \sim \Gamma(n, 1)$ , and the UL interference channel power gain is derived as  $g_{\text{MU}}^D = |h_{0,l}|^2 \sim \text{Exp}(1)$ .

For the typical SAP located at the origin  $\mathbf{0}$  in UL mode, the received SINR can be expressed as

$$\text{SINR}_U = \frac{Q_u r_0^{-\alpha} \|\mathbf{v}_0^\dagger \mathbf{g}_{0,0}\|^2}{I_U + |\mathbf{v}_0^\dagger \mathbf{n}_0|^2}, \quad (6)$$

where  $\mathbf{g}_{0,0} \in \mathbb{C}^{M \times 1}$  and  $\mathbf{v}_0 \in \mathbb{C}^{M \times 1}$ , respectively, denote the channel vector from the expected UL MU located at  $z_0$  to the typical SAP, and the unit norm ZF receive filter. The noise

power  $|\mathbf{v}_0^\dagger \mathbf{n}_0|^2 = \sigma^2$ , and the aggregated interference  $I_U$  is given by

$$\begin{aligned} I_U &= \sum_{n=1}^N \sum_{z_i \in \Phi_{u_n}^{\text{in}} \setminus \{z_0\}} Q_u \|z_{0,i}\|^{-\alpha} |\mathbf{v}_0^\dagger \mathbf{g}_{0,i}|^2 \\ &+ \sum_{k=1}^{\infty} \left[ \mathbf{1}_{\{\text{TX=U}\}}^{\text{out},k} \sum_{n=1}^N \sum_{z_m \in \Phi_{u_n}^{\text{out},k}} Q_u \|z_{0,m}\|^{-\alpha} |\mathbf{v}_0^\dagger \mathbf{g}_{0,m}|^2 \right. \\ &\left. + \mathbf{1}_{\{\text{TX=D}\}}^{\text{out},k} \sum_{n=1}^N \sum_{x_j \in \Phi_{s_n}^{\text{out},k}} P_s \|x_{0,j}\|^{-\alpha} |\mathbf{v}_0^\dagger \mathbf{H}_{0,j}^\dagger \mathbf{W}_j|^2 \right], \quad (7) \end{aligned}$$

where the first part, second part and last part denote the UL interference from intra-cluster zone, cross-cluster zone, and DL interference from cross-cluster zone, respectively. The symbols  $\mathbf{g}_{0,i} \in \mathbb{C}^{M \times 1}$  and  $\mathbf{H}_{0,j}^\dagger \in \mathbb{C}^{M \times M}$  denote the channel vectors from the interfering MU located at  $z_i$  and SAP located at  $x_j$  (to the typical SAP), respectively.

Let  $n_0 \in \{1, 2, \dots, N\}$  be the number of MUs associated with the typical UL SAP. By using ZF receiver, a unit norm receive filter  $\mathbf{v}_0 \in \mathbb{C}^{M \times 1}$  is selected orthogonal to the channel vectors of other  $n_0 - 1$  interferer associated with the same typical SAP, i.e.,  $|\mathbf{v}_0^\dagger \mathbf{g}_{0,p}|^2 = 0$  for  $p = 1, \dots, n_0 - 1$ .<sup>1</sup> As is derived in [19], we have  $h_{0,0}^U = \|\mathbf{v}_0^\dagger \mathbf{g}_{0,0}\|^2 \sim \Gamma(M - n_0 + 1, 1)$ ,  $g_{\text{MU}}^{\text{U,in}} = |\mathbf{v}_0^\dagger \mathbf{g}_{0,i}|^2 \sim \text{Exp}(1)$ ,  $g_{\text{MU}}^{\text{U,out}} = |\mathbf{v}_0^\dagger \mathbf{g}_{0,m}|^2 \sim \text{Exp}(1)$ , and  $g_{x_j, \text{SAP}}^U = |\mathbf{v}_0^\dagger \mathbf{H}_{0,j}^\dagger \mathbf{W}_j|^2 \sim \Gamma(n, 1)$ , respectively.

**Theorem 1.** *The DL and UL success probabilities of the typical SAP with  $n_0 \in \{1, 2, \dots, N\}$  associated MUs can be approximated by*

$$\begin{aligned} \mu_D(n_0) &\approx \int_0^\rho 2\pi \lambda_s r_0 \exp(-\pi \lambda_s r_0^2) \left[ \sum_{i=0}^{M-n_0} \frac{1}{i!} (-s)^i \right. \\ &\quad \left. \times \frac{d^i}{ds^i} \mathcal{L}_{I_{IN}^D}(s) \right]_{s=\frac{\gamma_D r_0^\alpha}{P_s}} dr_0, \quad (8) \end{aligned}$$

$$\begin{aligned} \mu_U(n_0) &\approx \int_0^\rho 2\pi \lambda_s r_0 \exp(-\pi \lambda_s r_0^2) \left[ \sum_{i=0}^{M-n_0} \frac{1}{i!} (-s)^i \right. \\ &\quad \left. \times \frac{d^i}{ds^i} \mathcal{L}_{I_{IN}^U}(s) \right]_{s=\frac{\gamma_U r_0^\alpha}{Q_u}} dr_0, \quad (9) \end{aligned}$$

where  $\mathcal{L}_{I_{IN}^D}(s)$  and  $\mathcal{L}_{I_{IN}^U}(s)$  are given by

$$\begin{aligned} &\mathcal{L}_{I_{IN}^D}(s) \\ &= \exp(-s\sigma^2) \exp\left\{-2\pi \sum_{n=1}^N \lambda_{s,n} \sum_{l=1}^n C_n^l \int_{r_0}^\rho \frac{(s P_s r^{-\alpha})^l r}{(1 + s P_s r^{-\alpha})^n} dr\right\} \\ &\times \prod_{k=1}^{\infty} \left\{ p_D \exp\left(-2\pi \sum_{n=1}^N \lambda_{s,n} \sum_{l=1}^n C_n^l \int_{\sqrt{k}\rho}^{\sqrt{k+1}\rho} \frac{(s P_s r^{-\alpha})^l r}{(1 + s P_s r^{-\alpha})^n} dr\right) \right. \\ &\quad \left. + (1 - p_D) \exp\left(-2\pi \sum_{n=1}^N \lambda_{u,n} \left( \Theta(\alpha, 1, (s Q_u)^{-1}, \sqrt{k+1}\rho) \right. \right. \right. \\ &\quad \left. \left. \left. - \Theta(\alpha, 1, (s Q_u)^{-1}, \sqrt{k}\rho) \right) \right) \right\}, \quad (10) \end{aligned}$$

<sup>1</sup>It is worth noting that when  $n_0 = 1$ , the ZF receiver becomes the maximal ratio combining (MRC) technique.

$$\begin{aligned}
& \mathcal{L}_{I_{IN}^U}(s) \\
&= \exp(-s\sigma^2) \exp\left(-2\pi \sum_{n=1}^N \lambda_{u,n} \Theta(\alpha, 1, (sQ_u)^{-1}, \rho)\right) \\
&\times \prod_{k=1}^{\infty} \left\{ p_D \exp\left(-2\pi \sum_{n=1}^N \lambda_{s,n} \sum_{l=1}^n C_n^l \int_{\sqrt{k}\rho}^{\sqrt{k+1}\rho} \frac{(sP_s r^{-\alpha})^l r}{(1+sP_s r^{-\alpha})^n} dr\right) \right. \\
&\quad \left. + (1-p_D) \exp\left(-2\pi \sum_{n=1}^N \lambda_{u,n} \left(\Theta(\alpha, 1, (sQ_u)^{-1}, \sqrt{k+1}\rho) \right. \right. \right. \\
&\quad \quad \left. \left. \left. - \Theta(\alpha, 1, (sQ_u)^{-1}, \sqrt{k}\rho)\right)\right)\right\} \quad (11)
\end{aligned}$$

with  $\lambda_{s,n} = \lambda_s f(n)$ ,  $\lambda_{u,n} = \lambda_s f(n) \cdot n$  and

$$\begin{aligned}
\Theta(\alpha, \beta, u, d) &\triangleq \int_0^d \frac{r^\beta}{1+ur^\alpha} dr \\
&= \frac{d^{\beta+1}}{\beta+1} {}_2F_1\left(1, \frac{\beta+1}{\alpha}; 1 + \frac{\beta+1}{\alpha}; -ud^\alpha\right)
\end{aligned}$$

with  ${}_2F_1(\cdot, \cdot; \cdot; \cdot)$  being the Gaussian hyper-geometric function.

*Proof:* See Appendix A.  $\square$

As can be seen from (8) and (9), the computation of  $\mu_D(n_0)$  and  $\mu_U(n_0)$  requires evaluating higher order derivatives of the Laplace transform. A larger parameter  $M - n_0$  leads to higher computational complexity. In the following corollary, we derive the upper bounds of  $\mu_D(n_0)$  and  $\mu_U(n_0)$  by employing the complementary cumulative distribution function (CCDF) of Gamma distribution.

**Corollary 1.** *The DL and UL success probabilities of the typical SAP with  $n_0 \in \{1, 2, \dots, N\}$  associated MUs are upper bounded by*

$$\begin{aligned}
\mu_D(n_0) &\leq \int_0^\rho 2\pi \lambda_s r_0 \exp(-\pi \lambda_s r_0^2) \left[ \sum_{i=1}^{\Delta_{n_0}} (-1)^{i+1} C_{\Delta_{n_0}}^i \right. \\
&\quad \left. \times \mathcal{L}_{I_{IN}^D}(i \cdot (\Gamma(\Delta_{n_0} + 1))^{-\frac{1}{\Delta_{n_0}} \cdot s}) \right]_{s=\frac{\gamma_D r_0^\alpha}{P_s}} dr_0, \quad (12)
\end{aligned}$$

$$\begin{aligned}
\mu_U(n_0) &\leq \int_0^\rho 2\pi \lambda_s r_0 \exp(-\pi \lambda_s r_0^2) \left[ \sum_{i=1}^{\Delta_{n_0}} (-1)^{i+1} C_{\Delta_{n_0}}^i \right. \\
&\quad \left. \times \mathcal{L}_{I_{IN}^U}(i \cdot (\Gamma(\Delta_{n_0} + 1))^{-\frac{1}{\Delta_{n_0}} \cdot s}) \right]_{s=\frac{\gamma_U r_0^\alpha}{Q_u}} dr_0, \quad (13)
\end{aligned}$$

where  $\Delta_{n_0} \triangleq M - n_0 + 1$ ,  $\mathcal{L}_{I_{IN}^D}(s)$  and  $\mathcal{L}_{I_{IN}^U}(s)$  are given by (10) and (11) in Theorem 1, respectively.

*Proof:* See Appendix B.  $\square$

With the law of total probability, the overall DL and UL success probabilities can be derived as

$$\mu_D = \sum_{n_0=1}^N \mu_D(n_0) f(n_0), \quad (14)$$

$$\mu_U = \sum_{n_0=1}^N \mu_U(n_0) f(n_0). \quad (15)$$

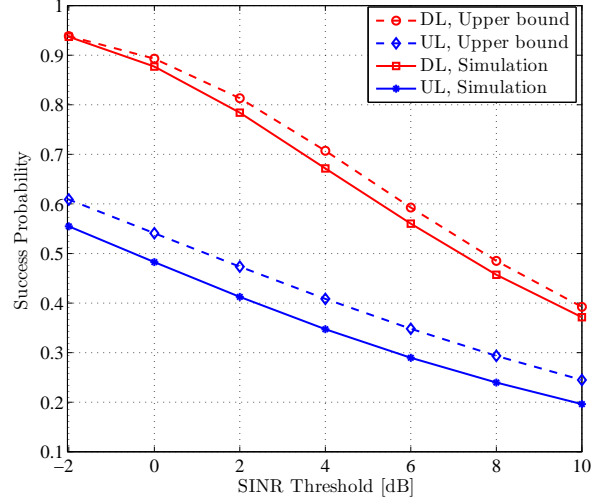


Figure 2. Success probability as a function of SINR threshold with cluster size  $l = 3$ , antenna number per SAP  $M = 8$ , and DL fraction  $p_D = 0.5$ .

## B. Network Throughput

With the success probability obtained above, we derive the network throughput of the small cell network in this subsection. Conditioned on the DL fraction  $p_D$  and the cluster size  $l$ , the DL and UL network throughput (in *Bits/Sec/Hz/m<sup>2</sup>*) can be written as

$$\mathcal{T}_D = p_D \lambda_s \log_2(1 + \gamma_D) \sum_{n_0=1}^N \mu_D(n_0) f(n_0) n_0, \quad (16)$$

$$\mathcal{T}_U = (1 - p_D) \lambda_s \log_2(1 + \gamma_U) \sum_{n_0=1}^N \mu_U(n_0) f(n_0) n_0. \quad (17)$$

## IV. NUMERICAL RESULTS

In this section, we first verify the theoretical model by means of simulations, and then provide key design insights for multi-antenna small cell networks under clustered D-TDD. We perform all simulations over a square window of  $1000 \times 1000$   $m^2$  with 10000 iterations. With the clustered D-TDD scheme, each SAP synchronizes its transmission to all the other SAPs within the same cluster, and serves all its associated MUs. Due to the high computational complexity of the analytical results derived in (8) and (9), in the following figures, we only plot the upper bound of the analytical results by using (12) and (13), respectively. Unless otherwise specified, we use the following default values of network parameters: SAP density  $\lambda_s = 10^{-3} m^{-2}$ , MU density  $\lambda_u = 10\lambda_s$ , transmit power of MU  $Q_u = 17$  dBm, maximum number of MUs associated to each SAP  $N = 3$ , and the number of antennas equipped by each SAP  $M = 8$ .

Figure 2 depicts the success probability as a function of SINR threshold. We observe that the upper bound of DL success probability is much tighter than that of UL success

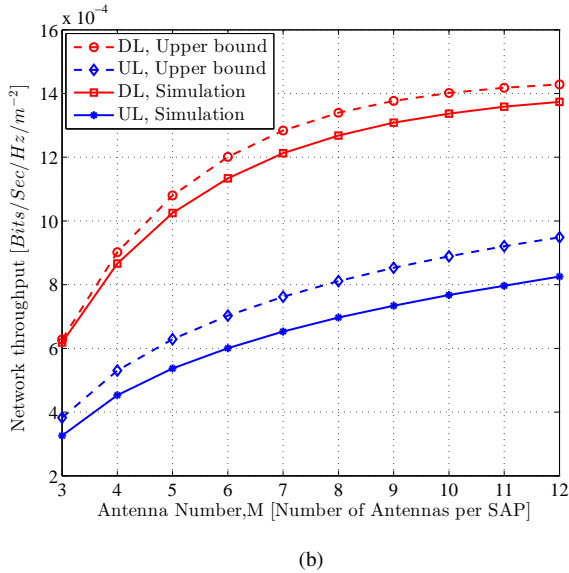
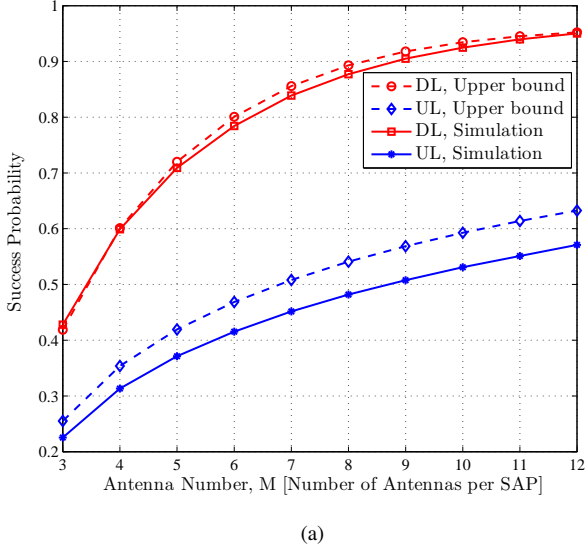


Figure 3. Success probability (a) and network throughput (b) as a function of SAP antenna number  $M$  with DL fraction  $p_D = 0.5$ , cluster size  $l = 3$ , and SINR threshold  $\gamma_D = \gamma_U = 0\text{dB}$ .

probability. This can be explained by the use of PPP approximation for active MUs in UL mode. Note that with the limitation on the maximum number of MUs  $N$  (associated with each SAP) and the DL fraction  $p_D$ , the active UL interfering MUs do not distribute as a PPP.

Figure 3 depicts the success probability and network throughput as a function of SAP antenna number  $M$  where the cluster size is set to be  $l = 3$ . From Fig. 3(a) and (b), we observe that an increasing antenna number of SAP  $M$  leads to an improvement in both success probability and network throughput. This can be explained by the enhanced spatial diversity gain achieved by each MU. With the number of served MUs  $N$  unchanged, a larger antenna number results in the higher transmit diversity.

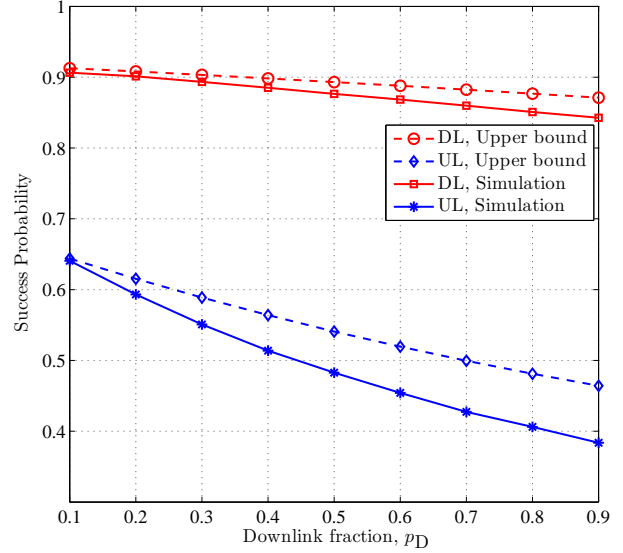
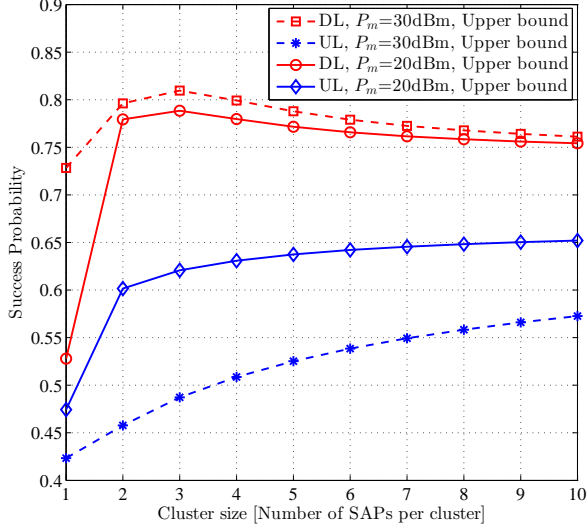


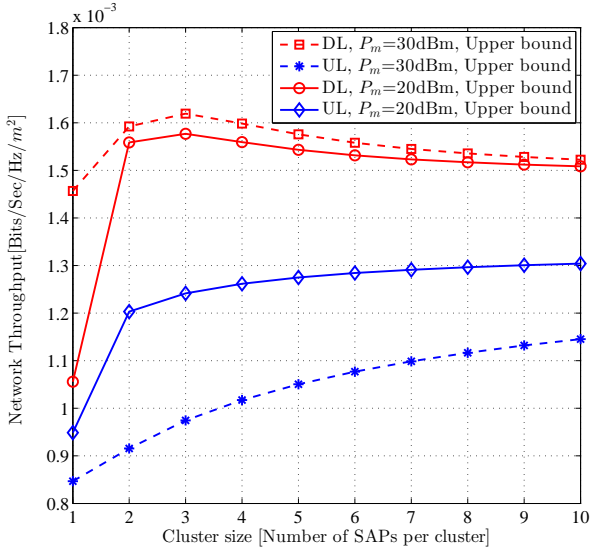
Figure 4. Success probability as a function of DL fraction  $p_D$  with cluster size  $l = 3$ , antenna number per SAP  $M = 8$ , and SINR threshold  $\gamma_D = \gamma_U = 0\text{dB}$ .

In Fig. 4, we plot the success probability as a function of DL fraction  $p_D$ . As  $p_D$  grows, the DL interfering SAP density increases while the UL interfering MU density decreases. With the considered parameter settings, it shows that both DL and UL success probabilities decrease with  $p_D$ . This can be explained by the huge difference in transmit power between SAP and MU, which results in the incremental aggregated interference.

Figure 5 depicts the success probability and network throughput as a function of cluster size  $l$ , i.e., the average number of SAPs per cluster, under different SAP transmit power. We observe that both success probability and network throughput in DL direction first grows and then decreases with respect to cluster size. This can be explained by the fact that when the cluster is small, the inter-cluster MU-to-MU interference dominates the DL transmission, and an enlargement of cluster eliminates the MU-to-MU interference, thus, boosting up the DL performance. However, as the cluster size keeps growing, the intra-cluster SAP-to-MU interference begins to dominate the DL transmission. As more and more SAPs are clustered and configured into the same direction, the increasing intra-cluster DL interference degrades the DL performance. Fig. 5 also shows that the UL performance always benefits from the growing cluster. This comes from the fact that the UL performance is dominated by the severe SAP-to-SAP interference, and an increase in cluster size helps eliminate the SAP-to-SAP interference, which improves the UL performance. What's more, a lower  $P_m$  leads to an enhancement in UL performance and a decrease in DL performance. Since  $l = 1$  corresponds to the traditional D-TDD scheme, Fig. 5(a) and (b) show the superiority of



(a)



(b)

Figure 5. Success probability (a) and network throughput (b) as a function of cluster size with antenna number per SAP  $M = 8$ , maximum number of MUs associated to each SAP  $N = 4$ , DL fraction  $p_D = 0.5$ , and SINR threshold  $\gamma_D = \gamma_U = 0\text{dB}$ .

clustered D-TDD scheme over the traditional D-TDD scheme in both success probability and network throughput. It further reveals that our proposed analytical framework can be used to determine the optimal cluster size (e.g.,  $l = 3$  in this example) for the DL performance.

## V. CONCLUSIONS

In this work, we proposed an analytical framework to investigate the network performance of multi-antenna D-TDD small cell network with cell clustering as the interference mitigation scheme. The framework allows to evaluate the

success probability and network throughput by accounting for the UL/DL configuration, cluster size, antenna number, transmit power, SINR threshold, and maximum number of MUs associated to each SAP. The superiority of the clustered D-TDD over the traditional D-TDD is revealed by numerical results. The proposed analytical framework can be used to find the optimal cluster size for the DL network performance, and it also revealed that a larger cluster size leads to better UL network performance.

## APPENDIX

### A. Proof of Theorem 1

The success probability  $\mu_{\text{TX}}$ ,  $\text{TX} \in \{\text{D}, \text{U}\}$  is affected by not only the interference, cluster size, but also the antenna number. For an SAP associating with  $n_0$  MUs, the DL success probability can be derived as

$$\begin{aligned} \mu_D(n_0) &\stackrel{(a)}{=} \int_0^\rho \Pr(h_{0,0}^D > s I_{IN}^D | n_0) f_r(r_0) dr_0 \\ &\stackrel{(b)}{=} \int_0^\rho \sum_{i=0}^{M-n_0} \frac{1}{i!} \mathbb{E}_{\{I_{IN}^D\}} [(s I_{IN}^D)^i e^{-s I_{IN}^D}] f_r(r_0) dr_0 \\ &\stackrel{(c)}{=} \int_0^\rho \sum_{i=0}^{M-n_0} \frac{1}{i!} (-s)^i \frac{d^i}{ds^i} \mathcal{L}_{I_{IN}^D}(s) \cdot f_r(r_0) dr_0, \end{aligned} \quad (18)$$

where  $\rho$  is cluster radius,  $f_r(r_0) = 2\pi\lambda_s r_0 \exp(-\pi\lambda_s r_0^2)$  is the PDF of the typical link length, and  $I_{IN}^D \triangleq I_D + \sigma^2$ . Step (a) is derived by defining  $s = \frac{\gamma_D r_0^\alpha}{P_s}$ , (b) follows from the CCDF of a Gamma variable  $X \sim \Gamma(k, \theta)$ , and (c) is derived by substituting  $\mathbb{E}_X[X^n e^{-sX}] = (-1)^n \frac{d^n}{ds^n} \mathcal{L}_X(s)$  and  $h_{0,0}^D \sim \Gamma(M - n_0 + 1, 1)$ .

To derive  $\mu_D(n_0)$ , we need to first calculate the  $i$ -th derivative of the Laplace transform of  $I_{IN}^D$ . Due to the independence of  $I_D$  and  $\sigma^2$ , we have  $\mathcal{L}_{I_{IN}^D}(s) = \mathbb{E}[e^{-s\sigma^2}] \mathcal{L}_{I_D}(s)$ . Conditioned on the typical link length  $r_0$ , the Laplace transform of  $I_D$  can be derived as

$$\begin{aligned} \mathcal{L}_{I_D}(s) &= \mathbb{E} \left[ \exp \left( -s \sum_{n=1}^N \sum_{x_i \in \Phi_{s_n}^{\text{in}} \setminus \{0\}} P_s \|x_{0,i}\|^{-\alpha} g_{\mathbf{x}_i, \text{SAP}}^D \right) \right. \\ &\quad \times \exp \left[ -s \sum_{k=1}^{\infty} \left( \sum_{n=1}^N \sum_{x_j \in \Phi_{s_n}^{\text{out}_k}} \mathbf{1}_{\{\text{TX}=\text{U}\}}^{\text{out}_k} P_s \|x_{0,j}\|^{-\alpha} g_{\mathbf{x}_j, \text{SAP}}^D \right. \right. \\ &\quad \left. \left. + \sum_{n=1}^N \sum_{z_l \in \Phi_{u_n}^{\text{out}_k}} \mathbf{1}_{\{\text{TX}=\text{U}\}}^{\text{out}_k} Q_u \|z_{0,l}\|^{-\alpha} g_{\mathbf{z}_l, \text{MU}}^D \right) \right] \Bigg] \\ &= \mathcal{L}_{I_D^{\text{in}}}(s) \cdot \mathcal{L}_{I_D^{\text{out}}}(s). \end{aligned} \quad (19)$$

Specifically, the Laplace transform of the intra-cluster interference  $I_D^{\text{in}}$  is given by

$$\begin{aligned} &\mathcal{L}_{I_D^{\text{in}}}(s) \\ &\stackrel{(a)}{=} \exp \left\{ - \sum_{n=1}^N \lambda_{s,n} \int_{\mathcal{C}(T,\rho) \setminus \mathcal{B}(0,x_0)} (1 - \mathcal{L}_{g_{\mathbf{x}_i, \text{SAP}}^D}(s P_s x^{-\alpha})) dx \right\} \\ &\stackrel{(b)}{=} \exp \left\{ -2\pi \sum_{n=1}^N \lambda_{s,n} \int_{r_0}^\rho \left( 1 - \frac{1}{(1 + s P_s r^{-\alpha})^n} \right) r dr \right\} \\ &\stackrel{(c)}{=} \exp \left\{ -2\pi \sum_{n=1}^N \lambda_{s,n} \sum_{l=1}^n C_n^l \int_{r_0}^\rho \frac{(s P_s r^{-\alpha})^l r}{(1 + s P_s r^{-\alpha})^n} dr \right\}, \end{aligned} \quad (20)$$

where  $g_{\mathbf{x}_i, \text{SAP}}^{\text{D}} \triangleq |\mathbf{h}_{0,i}^\dagger \mathbf{W}_i|^2$ , and  $\lambda_{s,n} = \lambda_s f(n)$ . Step (a) follows from the probability generating functional (PGFL) of PPP, (b) follows from the fact that  $g_{\mathbf{x}_i, \text{SAP}}^{\text{D}} \sim \Gamma(n, 1)$ , and (c) comes from Binomial theorem and the change from Cartesian to polar coordinates.

Similarly, the Laplace transform of the cross-cluster interference  $I_{\text{D}}^{\text{out}}$  is given by

$$\begin{aligned} & \mathcal{L}_{I_{\text{D}}^{\text{out}}}(s) \\ \stackrel{(a)}{\approx} & \prod_{k=1}^{\infty} \left\{ p_{\text{D}} \exp\left(-2\pi \sum_{n=1}^N \lambda_{s,n} \sum_{l=1}^n C_n^l \int_{\sqrt{k}\rho}^{\sqrt{k+1}\rho} \frac{(sP_s r^{-\alpha})^l r}{(1+sP_s r^{-\alpha})^n} dr\right) \right. \\ & \left. + (1-p_{\text{D}}) \exp\left(-2\pi \sum_{n=1}^N \lambda_{u,n} \left( \Theta(\alpha, 1, (sQ_u)^{-1}, \sqrt{k+1}\rho) \right. \right. \right. \\ & \left. \left. \left. - \Theta(\alpha, 1, (sQ_u)^{-1}, \sqrt{k}\rho) \right) \right) \right\}, \quad (21) \end{aligned}$$

where  $\lambda_{u,n} \approx \lambda_s n f(n)$ , and

$$\begin{aligned} \Theta(\alpha, \beta, u, d) & \triangleq \int_0^d \frac{r^\beta}{1+ur^\alpha} dr \\ & = \frac{d^{\beta+1}}{\beta+1} {}_2F_1\left(1, \frac{\beta+1}{\alpha}; 1 + \frac{\beta+1}{\alpha}; -ud^\alpha\right), \end{aligned}$$

with  ${}_2F_1(\cdot, \cdot; \cdot; \cdot)$  being the hypergeometric function. Note that the calculation of  $\lambda_{u,n}$  follows from the fact that there is a mapping between an SAP and its associated MUs. Assume an UL SAP associates with  $n$  MUs, then the density of interfering MUs is equivalent to  $\lambda_s n f(n)$ . Step (a) is due to the fact that all SAPs in each cluster are simultaneously configured in DL (resp. UL) with probability  $p_{\text{D}}$  (resp.  $1-p_{\text{D}}$ ), and the approximation of dividing the cross-cluster zone into a sequence of disjoint hexagonal rings.

Combining (20) with (21), we derive  $\mathcal{L}_{I_{\text{D}}^{\text{IN}}}(s)$  in (10). By substituting (10) into (18),  $\mu_{\text{D}}(n_0)$  is given by (8). Following the similar method, we derive  $\mu_{\text{U}}(n_0)$  in (9). This concludes the proof.

### B. Proof of Corollary 1

Define  $\gamma(m, z) = \int_0^z t^{m-1} e^{-t} dt$  as the lower incomplete Gamma function. The CCDF of Gamma distribution can be expressed as  $\bar{F}_Z(z) = 1 - \frac{\gamma(m, z)}{\Gamma(m)}$ . With Alzer's inequality in [20], we have

$$\frac{\gamma(m, z)}{\Gamma(m)} > (1 - \exp(-cz))^m. \quad (22)$$

For  $m > 1$ , we have  $c = (\Gamma(m+1))^{-\frac{1}{m}}$ . By expanding the expectation term, we have

$$\begin{aligned} \frac{\mathbb{E}_I[\gamma(m, zI)]}{\Gamma(m)} & \geq \mathbb{E}_I[(1 - \exp(-czI))^m] \\ & = \sum_{k=0}^m (-1)^k C_m^k \mathcal{L}_I(ckz). \quad (23) \end{aligned}$$

Take  $\mu_{\text{D}}(n_0)$  in (8) as an example, we have

$$\begin{aligned} & \sum_{i=0}^{M-n_0} \frac{1}{i!} (-s)^i \frac{d^i}{ds^i} \mathcal{L}_{I_{\text{D}}^{\text{IN}}}(s) \\ & = 1 - \frac{\mathbb{E}_{I_{\text{D}}^{\text{IN}}}[\gamma(M-n_0+1, sI_{\text{D}}^{\text{IN}})]}{\Gamma(M-n_0+1)} \end{aligned}$$

$$\begin{aligned} & \leq 1 - \sum_{i=0}^{\Delta_{n_0}} (-1)^i C_{\Delta_{n_0}}^i \mathcal{L}_{I_{\text{D}}^{\text{IN}}}(i \cdot (\Gamma(\Delta_{n_0}+1))^{-\frac{1}{\Delta_{n_0}}} s) \\ & \stackrel{(a)}{=} \sum_{i=1}^{\Delta_{n_0}} (-1)^{i+1} C_{\Delta_{n_0}}^i \mathcal{L}_{I_{\text{D}}^{\text{IN}}}(i \cdot (\Gamma(\Delta_{n_0}+1))^{-\frac{1}{\Delta_{n_0}}} s), \quad (24) \end{aligned}$$

where we define  $\Delta_{n_0} = M - n_0 + 1$  (a) follows from the fact that  $-(-1)^k = (-1)^{k+1}$  and that

$C_{M-n_0+1}^0 \mathcal{L}_{I_{\text{D}}^{\text{IN}}}(0) = 1$ . This concludes the proof.

### REFERENCES

- [1] N. Bhushan, J. Li, D. Malladi, R. Gilmore, D. Brenner, A. Damnjanovic, R. T. Sukhavasi, C. Patel, and S. Geirhofer, "Network densification: the dominant theme for wireless evolution into 5G," *IEEE Commun. Mag.*, vol. 52, no. 2, pp. 82–89, Feb. 2014.
- [2] A. Gotsis, S. Stefanatos, and A. Alexiou, "Ultradense networks: The new wireless frontier for enabling 5g access," *IEEE Veh. Technol. Mag.*, vol. 11, no. 2, pp. 71–78, 2016.
- [3] T. Q. S. Quek, G. de la Roche, I. Guvenc, and M. Kountouris, *Small Cell Networks: Deployment, PHY Techniques, and Resource Management*. Cambridge Univ. Press, 2013.
- [4] Q. Li, G. Li, W. Lee, M. il Lee, D. Mazzaresse, B. Clerckx, and Z. Li, "MIMO techniques in WiMAX and LTE: A feature overview," *IEEE Commun. Mag.*, vol. 48, no. 5, pp. 86–92, May 2010.
- [5] Z. Shen, A. Khoryaev, E. Eriksson, and X. Pan, "Dynamic uplink-downlink configuration and interference management in TD-LTE," *IEEE Commun. Mag.*, vol. 50, no. 11, pp. 51–59, Nov. 2012.
- [6] M. Ding, D. Lopez-Perez, R. Xue, A. V. Vasilakos, and W. Chen, "On Dynamic Time-Division-Duplex Transmissions for Small-Cell Networks," *IEEE Trans. Veh. Technol.*, vol. 65, no. 11, pp. 8933–8951, Nov. 2016.
- [7] H. Sun, M. Sheng, M. Wildemeersch, T. Q. S. Quek, and J. Li, "Traffic adaptation and energy efficiency for small cell networks with dynamic tdd," *IEEE J. Sel. Areas Commun.*, vol. 34, no. 12, pp. 3234–3251, 2016.
- [8] F. Sun and Y. Zhao, "Cell cluster-based dynamic TDD DL/UL reconfiguration in TD-LTE systems," in *Proc. IEEE WCNC*, April 2016, pp. 1–5.
- [9] D. Zhu and M. Lei, "Cluster-based dynamic DL/UL reconfiguration method in centralized RAN TDD with trellis exploration algorithm," in *IEEE Proc. WCNC*, Shang hai, China, Apr. 2013, pp. 3758–3763.
- [10] J. Li, A. Huang, H. Shan, H. H. Yang, and T. Q. S. Quek, "Analysis of Packet Throughput in Small Cell Networks Under Clustered Dynamic TDD," *IEEE Trans. Wireless Commun.*, vol. 17, no. 9, pp. 5729–5742, Sep. 2018.
- [11] Y. Zhong, T. Q. S. Quek, and X. Ge, "Heterogeneous cellular networks with spatio-temporal traffic: Delay analysis and scheduling," *IEEE J. Sel. Areas Commun.*, vol. 35, no. 6, pp. 1373–1386, 2017.
- [12] H. H. Yang, G. Geraci, Y. Zhong, and T. Q. S. Quek, "Packet Throughput Analysis of Static and Dynamic TDD in Small Cell Networks," *IEEE Wireless Commun. Lett.*, vol. 6, no. 6, pp. 742–745, Dec. 2017.
- [13] H. Sun, M. Wildemeersch, M. Sheng, and T. Q. S. Quek, "D2d enhanced heterogeneous cellular networks with dynamic tdd," *IEEE Trans. Wireless Commun.*, vol. 14, no. 8, pp. 4204–4218, 2015.
- [14] J. G. Andrews, F. Baccelli, and R. Ganti, "A tractable approach to coverage and rate in cellular networks," *IEEE Trans. Commun.*, vol. 59, no. 11, pp. 3122–3134, Nov. 2011.
- [15] M. Haenggi, *Stochastic Geometry for Wireless Networks*. Cambridge University Press, 2012.
- [16] J. Mecke, *Stochastic geometry and its applications*. Chichester: Wiley, 1995.
- [17] K. Huang and J. G. Andrews, "An analytical framework for multicell cooperation via stochastic geometry and large deviations," *IEEE Trans. Inf. Theory*, vol. 59, no. 4, pp. 2501–2516, April 2013.
- [18] H. Dhillon, M. Kountouris, and J. G. Andrews, "Downlink MIMO HetNets: Modeling, ordering results and performance analysis," *IEEE Trans. Wireless Commun.*, vol. 12, no. 10, pp. 5208–5222, Oct. 2013.
- [19] N. Jindal, J. G. Andrews, and S. Weber, "Multi-antenna communication in ad hoc networks: Achieving MIMO gains with SIMO transmission," *IEEE Trans. Commun.*, vol. 59, no. 2, pp. 529–540, February 2011.
- [20] H. Alzer, "On some inequalities for the incomplete gamma function," *Math. Comput.*, vol. 66, pp. 771–778, April 1997.